View metadata, citation and similar papers at core.ac.uk

brought to you by CORE

provided by University of Liverpool Repository

Tungsten 'fuzz' growth re-examined: The dependence on ion fluence in non-erosive and erosive helium plasma

T J Petty[1], M J Baldwin[2], M I Hasan[1], R P Doerner[2], and J W Bradley[1]

[1] Department of Electrical Engineering and Electronics, University of Liverpool, Brownlow Hill, Liverpool L69 3GJ, UK

[2] Center for Energy Research, University of California at San Diego, 9500 Gilman Dr, La Jolla, CA, 92093-0417, USA

E-mail: `j.w.bradley@liverpool.ac.uk`

Abstract. The thickness x, of tungsten fuzz layers are measured for non-varying helium (He) plasma exposure conditions spanning four orders of ion fluence Φ $\left(10^{24} - 10^{28}\ \mathrm{m^{-2}}\right)$ and flux Γ $\left(10^{19} - 10^{23}\ \mathrm{m^{-2}\ s^{-1}}\right)$, at $1000 - 1140$ K under low energy He ion impact $(50 - 80)$ eV. The data obtained are complemented by previously published data of similar growth conditions, and collectively analysed. The new analysis allows for the reconciliation of fast high flux growth with commonly observed slower growth at lower flux. It is demonstrated that the standing $t^{1/2}$ time dependence is a special case of a more general expression for determining the layer thickness, $x(\Phi) = (C(\Phi - \Phi_0))^{\frac{1}{2}}$, that depends on Φ, an incubation fluence Φ_0, and the growth constant $C = 2.36^{+1.54}_{-0.56} \times 10^{-38}\ \mathrm{m}^4$, which is temperature dependent. The incubation fluence, which must be exceeded before the observation on the onset of fuzz surface morphology is determined to be $\Phi_0 = 2.5^{+1.5}_{-1.0} \times 10^{24}\ \mathrm{m}^{-2}$. In fuzz growth-erosion regimes, characterized by an erosion constant ϵ_{fuzz}, that is proportional to the sputter yield, an analytic solution for $x(\Phi)$ has been found, by solving the growth-erosion equilibria problem of prior work with the Lambert W function. Simple limit expressions follow from the solution for determining the equilibrium fluence and fuzz thickness; the predictions of such being in good agreement with previous fuzz growth-erosion equilibria results in the literature.

1. Introduction

In recent years tungsten 'fuzz' has been actively researched [1–16] due to its potential formation in the ITER divertor, and likely presence in any DEMO reactor that utilizes tungsten armor. In ITER, fuzz formation might occur at the hottest parts (∼1000 K) of the tungsten strike points in view of the extensive observations of tungsten fuzz in these prior laboratory studies as well as in tokamak regimes [17, 18]. Although the literature highlights a greater number of positive aspects of tungsten fuzz than negative, the current view seems to be one of concern owing to almost no experience in dealing with a significant amount of fuzz at the plasma-material boundary in an actual fusion environment.

In a non or mildly erosive helium (He) plasma regime, tungsten fuzz is found to grow from bulk tungsten when simultaneously heated to ∼900-2000 K and bombarded by $> 20 - 30$ eV ions for a sufficient amount of time [1, 2]. This results in the original surface becoming deformed into a layer of nanoscopic branch-like structure with tendrils on the order of 50 nm wide, and an overall deformed layer thickness that can reach many μm [1]. The dependence of the fuzz layer thickness on plasma exposure time t, has been explored previously and determined to be more or less dependent on $t^{1/2}$ [1]. However, in that work the incident He ion flux was a constant. Later work [3, 4] shows that the same $t^{1/2}$ rate of growth is not maintained if the incident He ion flux is significantly less. In that case, many hours of plasma exposure under lower flux conditions are necessary to match layer thickness results taken at higher flux over just tens of minutes. This directly points to the additional importance of considering the total He ion fluence in addition to the observance of exposure time. Further, in [1] the quoted growth of the layer begins at the instant plasma is initiated. Later work suggests [5], and hints in experiment [6], that an amount of time is necessary for fuzz morphology to commence due to the need for prerequisite sub-surface He bubble formation and accumulation. This essentially amounts to an 'incubation' time or fluence, and is consistent with current hypotheses on the nature of fuzz growth [5, 19] that emphasize near surface He bubble formation as underpinning the fuzz growth process.

To reconcile prior issues surrounding fluence, flux, and time, an expanded set of fuzz layer growth data have been taken at ∼1120 K to complement the results in [1], which first demonstrated the $t^{1/2}$ nature of fuzz growth. The expanded set covers 4 orders of magnitude of He ion flux and fluence. The acquisition of these data necessitated the use of many plasma devices of differing plasma density and flux. Included are a magnetron device [4] at the University of Liverpool (UoL), an inductively coupled RF plasma device PISCES-E [20] and the DC reflex arc sources PISCES-A [21] and PISCES-B [22] located at the University of California at San Diego (UCSD). The new data obtained, as well as literature data taken under similar conditions, collectively give rise to a more general fluence dependent growth expression, which reduces to the $t^{1/2}$ dependent form of [1] for the special case of constant He ion flux and zero surface erosion. In erosive regimes, this new general expression is easily incorporated into the growth-erosion equilibria problem

of [7, 12]. This problem is solved mathematically to give an expression for defining the thickness of the tungsten fuzz layer under the competing processes of growth and recession by sputtering. A further outcome, in considering limits of this expression, is that simple analytical equations can be derived that give the approximate He ion fluence that satisfies the equilibria condition, and the equilibrium fuzz thickness, in an erosive regime. The validity of these simple expressions is explored by way of comparison to growth-erosion equilibrium results available in the literature and good agreement is observed.

2. Method

Four increasingly powerful plasma devices, each with successively overlapping parameter space, were used to examine the growth of tungsten fuzz over a wide range of He ion flux and fluence spanning four orders of magnitude. A comparative summary of the operational parameters is given in table 1. Full descriptions of each device can be found in the literature [4,20–22], but details pertinent to the current experiments are described.

Table 1. He plasma parameter spaces for the devices used in this study.

		UoL Mag.	Pisces-E RF	Pisces-A DC arc	Pisces-B DC arc
$P^*_{disch.}$	(kW)	0.7	1.3	1.5	3.0
Γ	(10^{22} $m^{-2}s^{-1}$)	0.001-0.02	0.01-0.5	0.5-8	5-20
$\Phi^\dagger$	(10^{26} m^{-2})	0.01-0.1	0.1-5	5-80	50-200
T^*_e	(eV)	∼7	∼4	∼6	∼6
n^*_e	(10^{18} m^{-3})	∼0.01	∼0.5	∼5	∼10

*Values of $P_{disch.}$ pertain to maximum Γ. Values of T_e and n_e are conditions at mid-range Γ.
†Calculated from ∼27 h (10^5 s) of exposure time.

The lowest He ion flux and fluence conditions were produced by a magnetron device at the UoL [4]. Samples exposed consisted of 99.95% tungsten discs, 10 mm in diameter and 1 mm thick. The sample surface was polished to a mirror-like finish with P1000 grade wet and dry emery paper and via electro-polishing. Following this, samples were exposed to He ions 100 mm away from a 150 mm dia. circular planar magnetron source operating with a He fill pressure of 5.3 Pa. The tungsten samples were held at a constant temperature using an e-beam heater and monitored with either a thermocouple or an IR pyrometer. A constant negative bias was applied to the sample, resulting in an average ion energy as displayed in table A1 by comparison to the plasma potential which was separately measured using an electrical probe. The thicknesses of the samples were determined by SEM inspection, in one case breaking the sample in half and viewing the cross-section, and the other by FIB milling out a trench and tilting the sample in an SEM.

UCSD tungsten fuzz layers were produced on tungsten sample discs of 20 mm dia. for use in Pisces-E and Pisces-A, and 25 mm dia. for use in Pisces-B. The tungsten stock was of 99.95% purity and all samples were 1.5 mm thick. Prior to plasma exposure, each was mechanically polished to a mirror finish down to a final lap with 3 μm diamond paste to produce a surface of average roughness better than 50 nm, as measured by a Tencor Alpha-Step profilometer. Three plasma devices were utilized at UCSD. These are the RF inductively coupled plasma source Pisces-E [20], and the two DC reflex arc sources Pisces-A [21] and Pisces-B [22]. In succession, these devices bridge the gap from the UoL magnetron device to fusion-edge-plasma relevant regimes, and thereby also provide the necessary connection between prior UoL [4] and UCSD [1] work.

Samples exposed in the Pisces-E device were kept fixed in temperature (measured by thermocouple) during He plasma exposure by externally applied resistive heating of the stage holding the sample. The sample was heated to $\sim$1100 K, and a He plasma was maintained for a set duration of time under constant conditions of RF power delivery at a frequency of 13.56 MHz. The sample was heated slightly by the plasma, but determined not to exceed 1150 K. He ion bombardment was established by the application of -65 V to the sample stage. A single RF electrical probe situated $\sim$10 mm from the sample was used to determine the plasma conditions. The plasma potential was measured at 15$\pm$5 V, giving the average energy of the bombarding He ions as $\sim$ 80 eV.

With the high density devices Pisces-A and Pisces-B, samples were heated by exposure to the plasma and the temperature was controlled by adjusting the flow rate of forced air cooling behind the sample. The temperature was measured by a thermocouple in contact with the back of the sample and kept fixed at $\sim$1140 K for each exposure. As the samples were heated by the plasma, exposure time was taken to begin when the sample temperature passes 1073 K, at which point cooling is increased until the temperature stabilizes at $\sim$1140 K. It is important to point out that the time taken to get from 973 K to 1073 K was 40$\pm$5 s, as fuzz is known to begin to grow around 900-950 K [2,6]. This 40 s is therefore used to establish a minimum error for the exposure fluence under low fluence operations, but is negligible for high fluence experiments in general. During exposure, samples were biased to -80 V, and a cylindrical reciprocating probe was momentarily inserted into the plasma in order to determine the He ion flux and plasma potential. The plasma potential was noted to be -6$\pm$1 V, thus giving an incident ion energy of $\sim$ 75 eV.

Subsequent to plasma exposure, the thicknesses of the fuzz layers was determined by cross-sectional scanning electron microscopy (SEM) and confocal laser microscopy (CFM). The SEM method is destructive to the sample, requiring a break to be made through the middle. We explore here, for the first time, a less destructive alternative approach using CFM. This requires only a very small scratch to be made on the fuzz surface with a sharp instrument that can not scratch the substrate bulk tungsten. Similar to that shown in [8], such a method effectively wipes the fuzz layer away at the scratch, to leave a trench that is only as deep as the fuzz layer. Under the CFM, which measures surface topography, the trench is clearly visible as shown in figure 1,

which also compares the same layer examined by cross-sectional SEM imaging. Both layer thicknesses are in agreement within error.

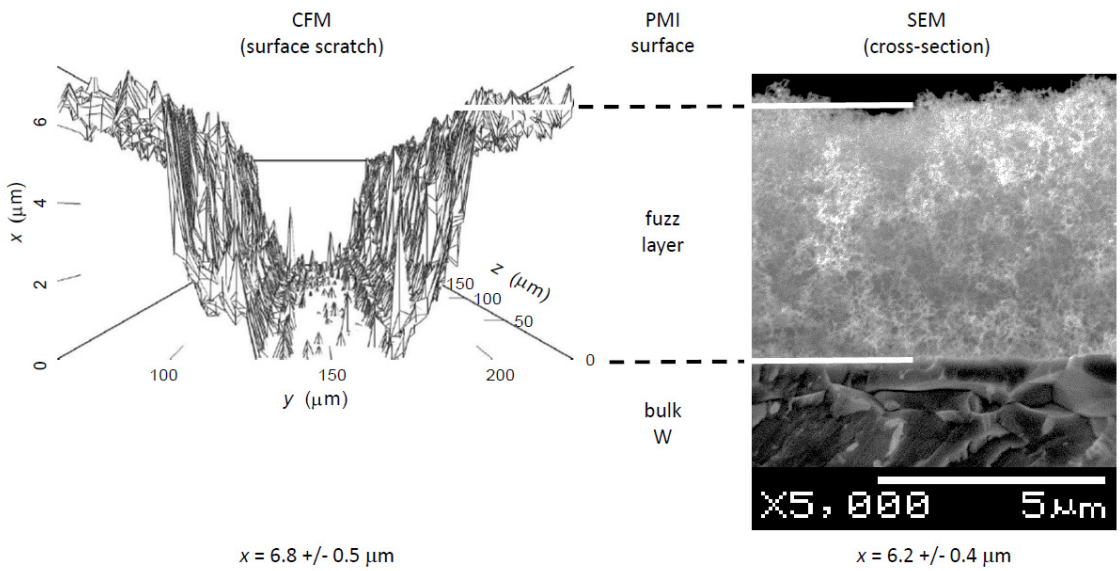

Figure 1. Comparison of tungsten fuzz layer thickness measured by CFM and cross-sectional SEM. The layer shown corresponds to the highest fluence exposed sample listed in table A1. Connecting lines highlight the plasma-material interaction (PMI) boundary and the tungsten fuzz-bulk interface, between both images.

3. Results

Sixteen samples of tungsten were exposed to He plasmas in the various devices described. For completeness, a listing of the plasma exposure conditions and subsequently measured fuzz layer thickness, are given in table A1. In addition to these data, a selection of tungsten fuzz results taken from the literature are listed in table A2, and are compiled to establish a database of available tungsten fuzz growth data at $\sim$1100$\pm$100 K. These results are used in conjunction with the current work. Additional work at the slightly higher temperature of 1400 K [2, 5, 23] was considered for inclusion, but due to known variation in fuzz growth rate with temperature [1], and higher temperature annealing effects [16], this work was not used in the current analysis. In establishing table A2 care was taken to measure fuzz layer thicknesses from only cross-sectional SEM images, and error bars assigned reflect the difficulty in determining the top of the fuzz layer and the boundary where fuzz grows from the substrate bulk. For each cited image, 5 measurements were obtained and an average value for the thickness determined.

4. Analysis and Discussion

The fuzz layer thickness data of this study, shown in table A1, and the compilation of table A2, are plotted (symbols) as a function of He ion fluence in figure 2. Corrections are applied to three of the current study data points. At low fluence, the data points produced in the magnetron device are revised lower in light of a measured mass gain caused by tungsten atom deposition [4] from the magnetron source. Due to the inherent nature of the magnetron device, there is a deposition flux of tungsten atoms on to the growing fuzz sample throughout the plasma exposure. The deposition rate was measured separately by a quartz crystal microbalance to be 5.3 $\pm$2.2 pm s^{-1}. Given the exposure time, this can be equated to a deposition layer and subtracted from the overall thickness, as shown in brackets in table A1. Since SEM observation of the fuzz morphology is similar to fuzz in other non UoL work, it is assumed that the deposited tungsten incorporates into the growing fuzz layer in a manner similar to that described by tungsten atom movement along tendrils, as proposed in [19]. The revision, which removes the influence of the deposition, places the data points closer to other nearby data that pertain to plasma exposure without an incident tungsten atom flux. The significance of this correction, however, should not be minimized. The uncorrected results are evidence that tungsten atom deposition leads to a potential enhancement of fuzz growth relative to non deposition regimes, and as such, warrants further investigation. Implications, for an all tungsten metal reactor scenario, are that tungsten codeposits might therefore manifest with fuzz like structure provided the requisite deposition temperature and He ion flux are also present.

The second revised data point is that taken at the highest He ion fluence (up to now) of $\Phi = 1.1 \times 10^{28}$ m^{-2} in Pisces-B. The measured fuzz layer thickness on this sample of $\sim$6.5 μm is depicted in figure 1, but according to a measured mass loss (2.01$\pm$0.01 mg) subsequent to exposure, the layer ought to have been $14.2\pm^{10.4}_{2.8}$ μm thick when corrected for fuzz porosity, which was measured to be 0.965 ± 0.02 using the method discussed in [8,10]. The error bars assigned to this data point (in figure 2) reflects the uncertainty in porosity, not mass loss (see Appendix C). In this case, in spite of the incident He ion energy being lower than necessary to cause sputtering, the discrepancy in the layer thickness is accountable by low level erosion of the fuzz layer by trace impurities ($<$ 0.01 %, N_2, O_2, W, etc) in the Pisces-B plasma acting over the almost 30 hours of plasma exposure time. The sputtering threshold energy for these impurities on tungsten is below the energy of the ions bombarding the sample during growth, hence erosion can occur this way [24].

Figure 2 also shows a straight line fit (dashed line) to the data. This line is related to the $t^{1/2}$ growth dependence given by Baldwin and Doerner [1], extrapolated over the expanded range of fuzz layer thickness data explored in this study. Originally, this dependence was stated as proportional to $t^{1/2}$ for the case of constant He ion flux, and given by

$$x = (2Dt)^{\frac{1}{2}}, \tag{1}$$

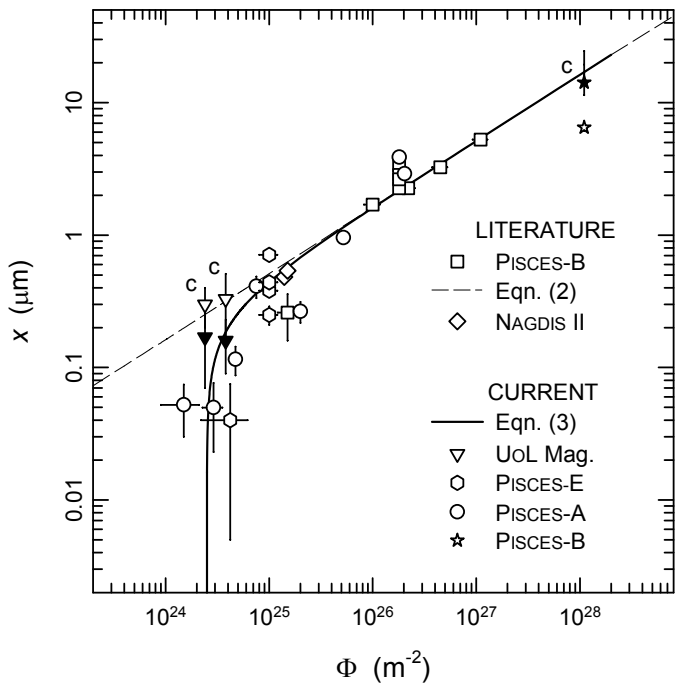

Figure 2. Fuzz layer thickness versus He ion fluence for data presented in tables A1 and A2. Literature value references are given in the tables. Where indicated, 'c' labels refer to corrected values. The dashed line is related to the $t^{1/2}$ growth dependence given by Baldwin and Doerner [1] extrapolated over the current expanded data set. The full line accommodates the effect of an incubation fluence of $\Phi_0 = 2.5 \times 10^{24}$ m^{-2} as described in the text.

where x is the thickness of the fuzz layer, D is the effective diffusion coefficient, and t is time. The transformation to fluence is straightforward [4], and carried out in figure 2 to facilitate comparison to layer thickness results at different ion fluxes. That is

$$x = (C\Phi)^{\frac{1}{2}}, \tag{2}$$

where Φ is the He ion fluence, $C = 2D/\Gamma$, and Γ is the He ion flux. The value of C at 1120 K is established readily from values given in [1], which quotes $D = 6.6 \times 10^{-16}$ m^{2}s^{-1} and the He ion flux at 5×10^{22} m^{-2}s^{-1}. It is thus determined that $C = 2.64 \times 10^{-38}$ m^4. It can be noted that over the extended range of He ion fluence the Baldwin and Doerner fit also reasonably describes most of the expanded set of data. The level of agreement between experiment and equation (2) over such a wide range of flux and fluence provides new insight. By normalizing the diffusion like constant D to the incident flux, thereby giving C, the more general expression of equation (2) resolves the interconnected role of He ion fluence, flux, and time in fuzz layer formation. This was not obvious in prior work involving the use of the constant D and shows the growth expression of [1] to be a special case of the more general expression of equation (2). However, it must be pointed out that while equation (2) agrees at least with currently available fuzz layer growth data, it is unclear if the same level of agreement extrapolates to fluences derived from extreme He ion flux $> 10^{23}$ m^{-2}s^{-1}, which lies beyond the scope of the present study.

There are also some differences between equation (2) and experiment that can be seen. In figure 2 it is evident that fuzz layer thickness increases rapidly to meet the fit (dashed line) at low fluence. In prior work, it has been suggested [5] and hinted at in experiment [6] that a certain amount of time ought to be necessary before fuzz layer growth can commence. In this time, an amount of He implants into the tungsten surface causing nanobubbles to form, that in turn, drive the onset and growth of the fuzz surface modification effect [5, 19]. On this basis the observed rapidly rising trend in fuzz layer growth is seemingly in agreement with the notion of an incubation fluence. The incubation effect is also noted in other works examining He in tungsten phenomena. For example, in [11], reduced optical properties of a polished tungsten surface exposed at >1000 K to He plasma in NAGDIS II was correlated with the formation of tungsten fuzz. Interestingly, no change was noted in the first minutes of exposure, until the He ion fluence reaches $\sim 2.4 \times 10^{24}$ m^{-2}. In another account [25], a He ion fluence of $\sim 10^{24}$ m^{-2} on tungsten is shown to lead to a He uptake of $\sim 5 \times 10^{20}$ m^{-2} in the near surface, and according to [26], this level of trapped He in the tungsten surface gives rise to the onset of a dense nanobubble field under examination by TEM. At lower retained He fluence the authors of [26, 27] note only platelet formation and dislocation loops; the precursor stages of bubble growth. The low fluence behavior of the fuzz layer thickness data in figure 2, is thus remarkably similar to that associated with the production of a near surface He bubble field found in earlier accounts. It is also worth mentioning, that a very similar level of He ion fluence leads to the onset of reduced D_2 retention in tungsten, which is associated with the formation of near surface He nanobubbles [28].

Including the effect of an incubation fluence, equation (2) can be rewritten as

$$x(\Phi) = \left(C(\Phi - \Phi_0)\right)^{\alpha}, \tag{3}$$

defined for $x(\Phi) : \Phi > \Phi_0$, and where $\alpha = \frac{1}{2}$ and Φ_0 is the minimum (incubation) He fluence required for fuzz morphology to be observed. Equation (3) is depicted in figure 2 by the full line for the case of $\Phi_0 = 2.5 \times 10^{24}$ m^{-2} and accommodates the trend in low fluence fuzz layer thickness data seemingly well.

The applicability of equation (3) is explored further by performing a constrained error analysis. Each parameter is varied to where the quality of the fit becomes poor while remaining parameters are re-optimized to obtain a measure of the uncertainties. This is shown in figure 3. Figure (3)(a) shows the effect of varying α. While it remains unclear as to precisely why α should be equal to 0.5 from a physics point of view, it remains the case that the data are best described by this value to within a $\pm 10\%$ variation. Based on this, the correctness of this value is therefore assumed in the absence of any physical model to the contrary. In the remainder of figure 3, other parameter optimizations, while fixing $\alpha = 0.5$, lead to the following fit values: $C = 2.36^{+1.54}_{-0.56} \times 10^{-38}$ m^4 and $\Phi_0 = 2.5^{+1.5}_{-1.0} \times 10^{24}$ m^{-2}.

Examining further the highest fluence data point, the lower than expected fuzz layer thickness is speculated to arise from low level impurity sputtering, which is consistent with the amount of measured mass loss. Yet while the precise nature of the loss remains

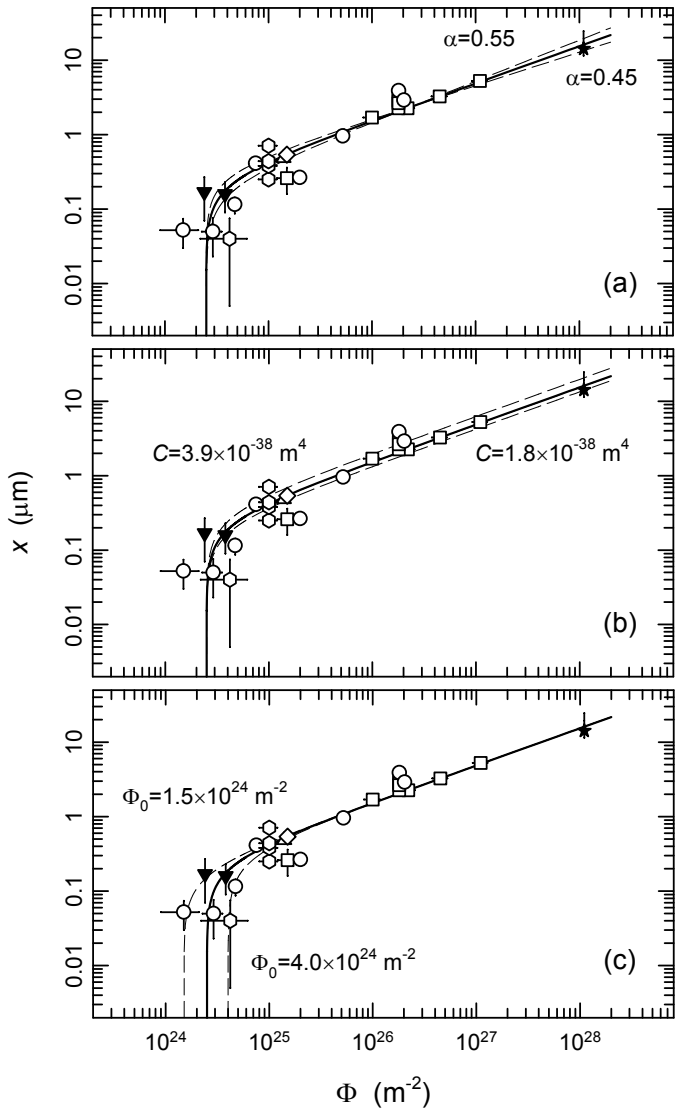

Figure 3. Optimizing equation (3) fitting parameters: (a) varying α and C, Φ_0 fixed (b) varying C, with α and Φ_0 fixed and (c) varying Φ_0, with C and α fixed. The full line is the optimized case where $\alpha = 0.5$, $\Phi_0 = 2.5 \times 10^{24}$ m^{-2} and $C = 2.36 \times 10^{-38}$ m^4. Dashed lines are the indicated parameter variations. See figure 2 caption for additional detail.

unclear, the measured mass reduction gives an effective fuzz erosion yield by the He plasma in spite of the below sputter threshold plasma regime. This yield can be used to corroborate the corrected value against growth erosion equilibria. Fuzz growth-erosion equilibrium has been studied by Doerner *et al.* [12] and more recently by Noiri *et al.* [7]. Both articles equate the derivative of the growth equation in [1] with an erosion velocity E, caused by sputtering. The erosion velocity E depends on flux. The growth rate equilibrium is defined by,

$$\frac{\mathrm{d}x}{\mathrm{d}t} = \frac{D}{x} - E = \frac{C\Gamma}{2x} - E. \tag{4}$$

Both computed [12] and numerical [7] solutions predict fuzz growth with time that

follows the time dependence in [1] until the forward growth rate of the fuzz is matched by the sputter erosion velocity. In terms of fluence, equation (4) is rewritten

$$\frac{\mathrm{d}x}{\mathrm{d}\Phi} = \frac{C}{2x} - \epsilon_{\mathrm{fuzz}}, \tag{5}$$

where $\epsilon_{\mathrm{fuzz}} = E/\Gamma$. Mathematically, there is a general solution to the differential problem in equation (5), which by direct integration is given as

$$x(\Phi) = \frac{C}{2\epsilon_{\mathrm{fuzz}}}\left(W\left[-\frac{1}{C}\exp\left(\frac{-2\epsilon_{\mathrm{fuzz}}^2}{C}(\Phi + \mathrm{A}) - 1\right)\right] + 1\right), \tag{6}$$

where A is the integration constant, and the function $W[z]$ acting on the real or complex argument z is the Lambert W or product-log function, which is well described in [29]. The constant A is found by applying the incubation fluence boundary condition $x(\Phi_0) = 0$, which is only satisfied when the W function is equal to -1, meaning that its argument, by definition, is equal to $-\mathrm{e}^{-1}$. It is thus straightforward to show that $\mathrm{A} = -\left(C \ln C\right) / \left(2\epsilon_{\mathrm{fuzz}}^2\right) - \Phi_0$. Substituting this back into (6) leads to the general solution

$$x(\Phi) = \frac{C}{2\epsilon_{\mathrm{fuzz}}}\left(W\left[-\exp\left(-\frac{2\epsilon_{\mathrm{fuzz}}^2}{C}(\Phi - \Phi_0) - 1\right)\right] + 1\right), \tag{7}$$

which gives the thickness of a tungsten fuzz layer in an erosive regime characterized by ϵ_{fuzz}, as a function of the He ion exposure fluence. There are several interesting features to be noted. First, in the limit $\Phi \to \infty$ the exponential term tends to 0, and since $W[0] = 0$, $x(\Phi) \to C/2\epsilon_{\mathrm{fuzz}}$. That is, $x(\Phi)$ approaches a constant equilibrium thickness defined by just the growth constant C and the erosion constant ϵ_{fuzz}; neither of which depend on flux. In the second instance, an indeterminate nature of the solution appears when the erosion constant ϵ_{fuzz} is zero. In this case, equation (3) should be used. However, in the interest of completeness, it is shown that equation (7) converges to equation (3) in the limit as $\epsilon_{\mathrm{fuzz}} \to 0$ in Appendix B. Lastly, as with equation (3), real solutions only occur when $\Phi > \Phi_0$. Figure 4 is a reproduction of figure 2, but with an overlay of equation (7) using a value of $\epsilon_{\mathrm{fuzz}} = 1.69 \times 10^{-33}$ m^3 (See also table 2.). It can be seen that equation (7) deviates from the original fit of (3) at higher fluence to accommodate the measured fuzz erosion of the highest fluence sample.

The erosion constant ϵ_{fuzz} can be determined as follows: the rate of removal of tungsten atoms per unit area, in units of atoms$\cdot$m^{-2}s^{-1}, is given by $Y_{\mathrm{bulk}}\Gamma$, where Y_{bulk} is the bulk tungsten sputter yield [24]. This constitutes an erosion velocity E (as defined previously) into the surface in ms^{-1}. The proportionality between these two quantities is $\kappa = \mathrm{m_W}/\rho_{\mathrm{W}}$ where $\mathrm{m_W}$ is the mass of the tungsten atom and ρ_{W} is the density. That is

$$\epsilon_{\mathrm{bulk}} = \kappa Y_{\mathrm{bulk}}. \tag{8}$$

However, for a fuzz surface the effect of porosity must be included and its influence reduces both the yield and the overall density. Following [10], we denote the porosity of the tungsten fuzz as p, and utilize the fact that to good approximation, the term

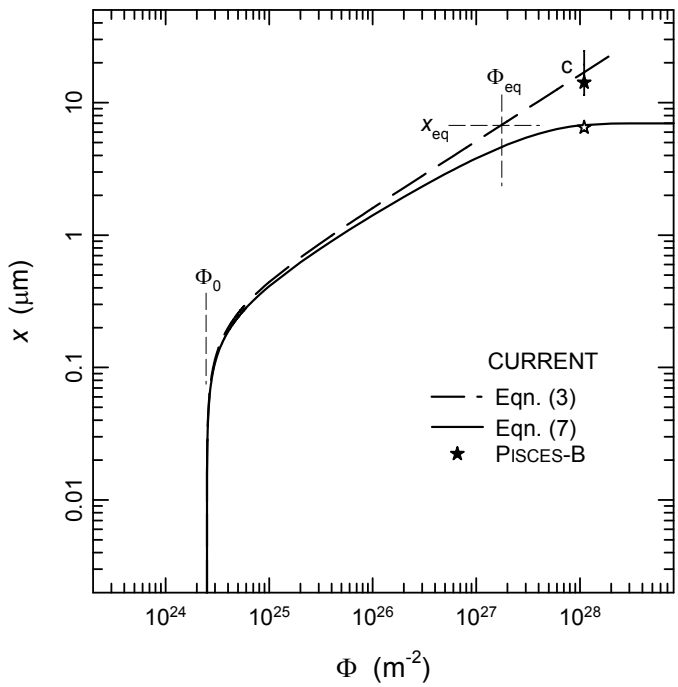

Figure 4. Similar to figure 2, but showing comparison of the general growth-erosion expression (7), and equation (3). The fuzz layer thickness for the corrected (filled-in star) and uncorrected (eroded) highest fluence sample (open star) is also shown, as is described at the beginning of section 4. In calculation, $C = 2.36\times10^{-38}$ m^4 and $\epsilon_{\rm fuzz} = 1.69 \times 10^{-33}$ m^3, determined from a fuzz porosity of $p = 0.985$ [10]. In this figure $x_{\rm eq}$, $\Phi_{\rm eq}$ and Φ_0 are indicated as per description in the text. See also table 2 and figure 2 caption for additional detail.

$(1-p)$ varies directly with the the sputter yield of fuzz relative to bulk tungsten. That is, $Y_{\rm fuzz} \approx (1-p)\, Y_{\rm bulk}$ (see Appendix C). Likewise for the bulk tungsten density, it is reduced (at least macroscopically) by the same factor of $(1-p)$. Thus, for the erosion of fuzz:

$$\epsilon_{\rm fuzz} \approx \kappa \frac{(1-p)}{(1-p)} Y_{\rm bulk}, \qquad \epsilon_{\rm fuzz} \approx \kappa \frac{1}{(1-p)} Y_{\rm fuzz}. \tag{9}$$

Accordingly, if the yield is taken from measurements or predictions [24] of the sputter yield made for bulk tungsten ($Y_{\rm bulk}$), the porosity term cancels and $\epsilon_{\rm fuzz} = \epsilon_{\rm bulk}$, as was demonstrated recently in [7]. On the other hand, if the erosion yield is determined from experiment ($Y_{\rm fuzz}$), as is the case here and in [12], $\epsilon_{\rm fuzz}$ must be calculated by including the porosity of the fuzz layer.

Substituting equation (9) into the equilibrium thickness limit $C/2\epsilon_{\rm fuzz}$ leads to:

$$x_{\rm eq} \approx C\left(\frac{1}{2\kappa Y_{\rm bulk}}\right), \qquad x_{\rm eq} \approx C\left(\frac{1-p}{2\kappa Y_{\rm fuzz}}\right), \tag{10}$$

where the equilibrium thickness $x_{\rm eq}$ is expressed in terms of both bulk, and fuzz, tungsten erosion yields. Similarly, it is relatively simple to further show that the approximate ion

fluence $\Phi_{\rm eq}$, necessary to approach the equilibrium condition is:

$$\Phi_{\rm eq} \approx C\left(\frac{1}{2\kappa Y_{\rm bulk}}\right)^2 + \Phi_0, \qquad \Phi_{\rm eq} \approx C\left(\frac{1-p}{2\kappa Y_{\rm fuzz}}\right)^2 + \Phi_0, \tag{11}$$

whereby equation (10) is solved with equation (3). Both $x_{\rm eq}$ and $\Phi_{\rm eq}$ are shown geometrically in figure 4. Taken together, equations (10) and (11) are useful 'rule of thumb' expressions for determining the equilibrium fluence and thickness for tungsten fuzz layers in growth-erosion regimes. However, it must be emphasized that equation (10) is only reliable for $\Phi > \Phi_{\rm eq}$, which can be checked using equation (11). Otherwise, for the case $\Phi < \Phi_{\rm eq}$, the fuzz layer thickness can only be accurately found using equation (7) as depicted in figure 4.

Table 2. Comparison of current and literature fuzz layer thickness results in growth-erosion regimes.

Ref.	Φ	T*	$E_{\rm ion}$	$Y_{\rm fuzz}$ (meas.)	$Y^{\dagger}_{\rm bulk}$ [24]	p [10]	x (meas.)	$x(\Phi)$ Eqn.(7)	$x_{\rm eq}$ Eqn.(10)	$\Phi_{\rm eq}$ Eqn.(11)
	(10^{26} m^{-2})	(K)	(eV)	(10^{-3})	(10^{-3})		(μm)	(μm)	(μm)	(10^{26} m^{-2})
	110	1140	75	0.0016	–	0.945 – 0.985	6.5±0.5	6.8 – 12.9	7.0 – 25.6	21 – 280
[12]	3.6	1120	200	–	2.3	–	2.0±0.5	1.5	1.6	1.1
[12]	3.6	1120	200	0.15	–	0.85 – 0.95	2.0±0.5	0.2 – 0.7	0.2 – 0.7	0.05 – 0.26
[12]	3.6	1120	250	–	5.4	–	0.9±0.3	0.7	0.7	0.2
[12]	3.6	1120	250	0.34	–	0.75 – 0.90	0.9±0.3	0.2 – 0.5	0.2 – 0.5	0.05 – 0.15
[7]	0.3	1300	250	–	5.4	–	2.0±0.5	1.0	1.9	0.6
[7]	0.03‡	1300	400	–	15	–	0.7±0.2	0.3	0.7	0.09
[7]	0.2	1300	400	–	15	–	0.7±0.2	0.6	0.7	0.1
[7]	0.02‡	1300	500	–	20	–	0.4±0.1	0.2	0.5	0.05
[7]	0.3	1300	500	–	20	–	0.3±0.1	0.5	0.5	0.06

*C is taken to be 2.36×10^{-38} m^4 at 1120 K (present study). To accommodate exposure temperature other than the present study, the temperature dependence in [1] is used to adjust C.

†In equations (7) (10) and (11) when yield values of [24] are used, $Y_{\rm bulk}$ is reduced by a factor of 5 as described in the text.

‡For these low fluence cases Φ_0 was taken to be the minimum at 1.5×10^{24}m^{-2}. For all other cases Φ_0 was taken as 2.5×10^{24}m^{-2}.

Equation (7) and the limit expression (10) are explored further by application to other fuzz growth-erosion cases in the literature. The results are tabulated in table 2, which also shows the current growth-erosion case. As can be seen, predicted and experimental values are in reasonable agreement over a wide range of cases of differing He ion fluence, ion impact energy, and exposure temperature. Although, by inspection of the measured values of x against calculated values of $x(\Phi)$, it is clear that accuracy is favored by avoiding the use of measured fuzz yields, and thus the need to account for porosity, which introduces a large uncertainty in calculated results for only slight

variation. Better agreement is apparent for the use of bulk yields, but it is emphasized that the yield values of [24] in table 2 were systematically reduced by a further factor of 5 in calculations to achieve such agreement. This was done in accordance with the well known discrepancy [30, 31] that exists between sputter yields obtained in high flux plasma experiments and calculations, whenever low mass projectile species (D, He) are involved.

Figure 5 shows plots of the limit expressions (10) and (11) as a function of erosion yield Y, for variation of exposure temperature using the temperature dependence given in [1]. The growth erosion cases of table 2 are overlaid for comparison and demonstrate the effective simplicity of these equations in determining equilibrium fuzz growth-erosion fluence and thickness. To reiterate, once it is determined that a specific level of plasma exposure exceeds $\Phi_{\rm eq}$, as in figure 5(a), $x_{\rm eq}$ can be reliably deduced, such as in figure 5(b).

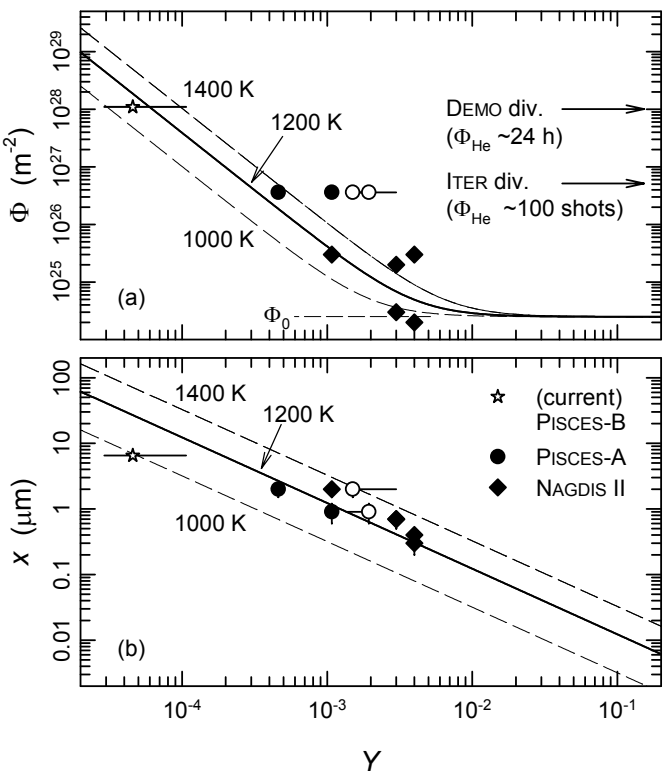

Figure 5. Plot of (a) $\Phi_{\rm eq}$ and (b) $x_{\rm eq}$, as a function of erosion yield Y, produced from equations (10) and (11). Full and dashed lines correspond to adjusted C values corresponding to 1000, 1200, and 1400 K, using the temperature dependence in [1]. Overlaid data points are fuzz layer thicknesses corresponding to the erosion regimes and references of table 2. Open symbols pertain to cases with measured fuzz yields and to compare to line plots $Y_{\rm fuzz}/(1-p)$ is used for the abscissa. Similarly, full symbols are those of bulk yields. To compare these the abscissa is $Y_{\rm bulk}/5$. See table 2 footnotes.

In these plots the estimated He fluence for the ITER and DEMO divertor are given for 100 shots and 24 h respectively [32,33] and suggest that a growth-erosion equilibrium

should be reached well within these times frames if the sputter yield is kept close to, or below threshold. According to [34], the net ITER tungsten fuzz erosion rate is predicted to be $\sim 3 \times 10^{-10}$ ms^{-1} which is closely similar to the highest fluence case reported here. The equilibrium thickness, x_{eq}, can be estimated by $x_{\mathrm{eq}} = C/2\epsilon_{\mathrm{f}}$, with $\epsilon_{\mathrm{f}} = \mathrm{E}/\Gamma$. Brooks *et al.* [32] predict the D-T flux in the divertor region to be $\sim 4 \times 10^{23}$ m^{-2}s^{-1}, of this flux 5% is He, hence Γ_{He} is $\sim 2{\times}10^{22}$ m^{-2}s^{-1}. Keeping to the fuzz created in a similar temperature window as the PISCES-B sample here, i.e. $C = 2.36 \times 10^{-38}$ m^4, which is a fair assumption given the hottest parts of the W divertor region are expected to be 1000 - 1400 K [35], this gives $x_{\mathrm{eq}} = 0.8$ μm. This is much lower than in PISCES-B due to an order of magnitude lower He ion flux but a similar erosion rate, hence equilibrium will be reached at lower thickness.

It is difficult to extrapolate to the case for DEMO, though one might speculate similar levels of erosion based on flux estimates [36], that nevertheless lead to similar levels of equilibrium fuzz thickness. This means that in a reactor scenario, the growth of the fuzz layer will likely be limited in both eroding and non eroding (by impurities or other) regimes to the micron scale by growth-erosion equilibria, and overall erosion should be low since the porosity of the structure produces a considerably reduced erosion yield compared with bulk tungsten. Further, the UoL magnetron result suggests that any eroded tungsten may act to re-integrate with existing fuzz at deposition locations, but further work must be done to investigate this effect in a systematic manner and any potential impact on the growth-erosion equilibria.

5. Conclusions

The thickness of tungsten fuzz layers has been measured across four orders of magnitude of He ion fluence and flux under below threshold sputtering conditions in the temperature range of $1000 - 1140$ K and compared to a compilation of previously published data. Considering the growth of the layer as a function of the He ion fluence (rather than time) reveals a more general form of the growth dependence than was originally given in [1] and reconciles different rates of growth observed at different fluxes. The current analysis shows that the dependence in [1] is a special case of the more general growth expression of equation (3), which also accommodates the observation of a rapid onset of early stage growth by the inclusion of an incubation fluence. Arguments are made that the incubation fluence is almost certain to be associated with the set up formation of a He nanobubble field within the near surface. The general growth expression is easily incorporated into the growth-erosion equilibrium problem of [7, 12] to give an analytical solution based on the Lambert W function, and for which simple 'rule of thumb' limit expressions can be derived to determine the equilibrium thickness and approximate equilibrium fluence from a specified erosion yield.

Acknowledgements

The authors would like to thank Michael Simmonds, Dr. Ionut Jepu, and Alan Roby for their assistance in this investigation, and Tyler Lynch for sample preparation. Mr Petty would like to gratefully acknowledge the University of Liverpool for his studentship, supported by the Engineering and Physical Sciences Research Council (EPSRC) doctoral training grant (Fusion DTC). This work was also supported by US DoE Grant Award: #DE-FG02-07ER54912.

Appendix A

Table A1. Plasma conditions and fuzz layer thicknesses in this study.

Device	Φ	Γ	T	E_i	x
	(10^{26} m^{-2})	(10^{22} m^{-2}s^{-1})	(K)	(eV)	(μm)
UoL Mag.	0.024±0.0002	0.010±0.0005	1000±50	56.5	0.3±0.1
					(0.17±0.10)*
	0.038±0.0002	0.012±0.0002	1100±50	59.5	0.33±0.18
					(0.16±0.07)*
Pisces-E	0.04±0.02	0.20±0.04	1100±50	80	0.04±0.03
	0.10±0.02	0.19±0.04	1100±50	80	0.25±0.04
	0.10±0.02	0.19±0.04	1100±50	80	0.38±0.03
	0.10±0.02	0.19±0.04	1100±50	80	0.44±0.05
	0.10±0.02	0.19±0.04	1100±50	80	0.71±0.06
Pisces-A	0.015±0.006	1.4±0.04	1140±20	75	0.05±0.03
	0.028±0.006	1.4±0.04	1140±20	75	0.05±0.03
	0.047±0.005	1.7±0.40	1140±20	75	0.12±0.04
	0.075±0.007	1.5±0.04	1140±20	75	0.41±0.08
	0.20±0.01	1.4±0.04	1140±20	75	0.27±0.05
	0.52±0.02	1.0±0.04	1140±20	75	0.96±0.16
	1.81±0.21	2.0±0.24	1140±20	75	3.87±0.16
	2.03±0.12	1.9±0.12	1140±20	75	2.90±0.20
Pisces-B	110.0±10	11.00±1	1120±30	75	6.5±0.4
					$\left(14.2\pm^{10.4}_{2.8}\right)^*$

*Bracketed values are corrected for either mass gain or loss during plasma exposure as described in the text.

Table A2. Literature fuzz layer thicknesses for below sputter threshold He plasma exposure in the temperature range of 1000 − 1200 K.

Ref.	Fig.	Device	$\Phi^\dagger$	Γ	T	E_i	x
			(10^{26} m^{-2})	(10^{22} m^{-2}s^{-1})	(K)	(eV)	(μm)
[1]	3a	Pisces-B	0.15±0.03	5.0	1120	60	0.26±0.1
	3b		1.0±0.18	5.0	1120	60	1.70±0.1
	3c		2.2±0.36	5.0	1120	60	2.64±0.1
	3d		4.5±0.75	5.0	1120	60	3.25±0.1
	3e		11.0±1.8	5.0	1120	60	5.26±0.1
[8]	2b	Pisces-B	1.8	5.0	1120	60	3.35±0.45
	5a		1.8	5.0	1120	40	2.85±0.17
	5c		1.8	5.0	1120	40	2.64±0.24
[17]	2b	Nagdis	0.14	1.0	1070	50	0.48±0.06
[11]	6a	Nagdis II	0.15	0.8	∼1200	50	0.54±0.06

†Where provided, uncertainties are taken from listed Ref.

Appendix B

The integral solution of equation (5) for $x(\Phi) : \Phi > \Phi_0$ and boundary condition $x(\Phi_0) = 0$ applied, is given by equation (7) and reproduced below for convenience

$$x(\Phi) = \frac{C}{2\epsilon_{\text{fuzz}}}\left(W\left[-\exp\left(-\frac{2\epsilon_{\text{fuzz}}^2}{C}(\Phi - \Phi_0) - 1\right)\right] + 1\right). \tag{B.1}$$

This equation is problematic in that the solution is indeterminate when $\epsilon_{\text{fuzz}} = 0$. However, it ought to converge to the non erosion fluence dependent equation (3) in the limit $\epsilon_{\text{fuzz}} \to 0$. Using approximation methods it is shown that this is indeed the case. If a substitution of variable is made such that $\beta = \exp\left(-2\epsilon_{\text{fuzz}}^2(\Phi - \Phi_0)/C\right)$, the argument of the W fuction in equation (B.1) becomes $-\beta \mathrm{e}^{-1}$. Following the methodology in [37], the W function can be expanded by power series to give

$$W[-\beta \mathrm{e}^{-1}] = -1 + \sqrt{2(1-\beta)} - \frac{2}{3}(1-\beta) + ... \quad . \tag{B.2}$$

As the series expands, the factor $(1 - \beta)$ increases in power by a factor of $\frac{1}{2}$ for each additional term, but as $\epsilon_{\text{fuzz}} \to 0$, $\beta \to 1$, meaning that higher order terms become increasingly small. We therefore truncate the expression to the first two terms. In a similar fashion, a Taylor series expansion can be performed on β

$$\beta = 1 - \frac{2\epsilon_{\text{fuzz}}^2}{C}(\Phi - \Phi_0) + \left(\frac{2\epsilon_{\text{fuzz}}^2}{C}(\Phi - \Phi_0)\right)^2 - ... \quad , \tag{B.3}$$

where again, as $\epsilon_{\text{fuzz}} \to 0$, the higher order terms are increasingly small. Substituting this expression, again truncated to two terms, into (B.2) gives (for small $\epsilon_{\text{fuzz}} \to 0$)

$$W[-\beta \mathrm{e}^{-1}] \approx -1 + \left(\frac{4\epsilon_{\text{fuzz}}^2}{C}\left(\Phi - \Phi_0\right)\right)^{\frac{1}{2}} \tag{B.4}$$

Substituting the result of equation (B.4) into (B.1) results in equation (B.5), or the approximation of equation (3).

$$x(\Phi) \approx \left(C(\Phi - \Phi_0)\right)^{\frac{1}{2}}. \tag{B.5}$$

Appendix C

The equations in 9 show how to obtain the fuzz erosion constant ϵ_{fuzz}, from bulk [24] and experimentally measured yield values. For the case where a bulk yield is used the porosity p, of the layer is unimportant as the term $(1-p)$ cancels. This is noted in a previous article by Noiri *et al.* [7], where eroded fuzz thickness is best explained by TRIM yields in [24]. For the case where the fuzz erosion yield is measured, such as in Doerner *et al.* [12], the porosity must be considered since fuzz erosion yields are always significantly lower than that for bulk tungsten [10]. Following [10], the close variation of fuzz erosion yield compared to bulk tungsten $Y_{\text{fuzz}}/Y_{\text{bulk}}$, and $(1-p)$, is therefore used in equations 9, 10 and 11, and table 2, to essentially correct for the low fuzz yield. For completeness, we reproduce the results of [10] in figure C1. This figure is a re-plotting of figure 6(a) in that article, with a few more recent data added, and demonstrates the experimentally determined relationship (crosses) between $Y_{\text{fuzz}}/Y_{\text{bulk}}$ and the porosity term $(1-p)$. The full line is an overlay of $Y_{\text{fuzz}}/Y_{\text{bulk}} = (1-p)$. The lighter long-dashed line is a weighted linear regression (coefficient of determination, $r^2 = 0.95$) and closely approximates the full line. The data (triangles) show corresponding measurements of fuzz layer thickness x, versus $(1-p)$. The dashed line is a hyperbola fit used only to guide the eye. In the analysis of table 2, the large range for error in row calculations, where measured fuzz yields are used, stems from the increased uncertainty in the term $(1-p)$ for thicker layers with higher porosity. It is left to the reader, in their own experiments, to decide a sufficient level of accuracy.

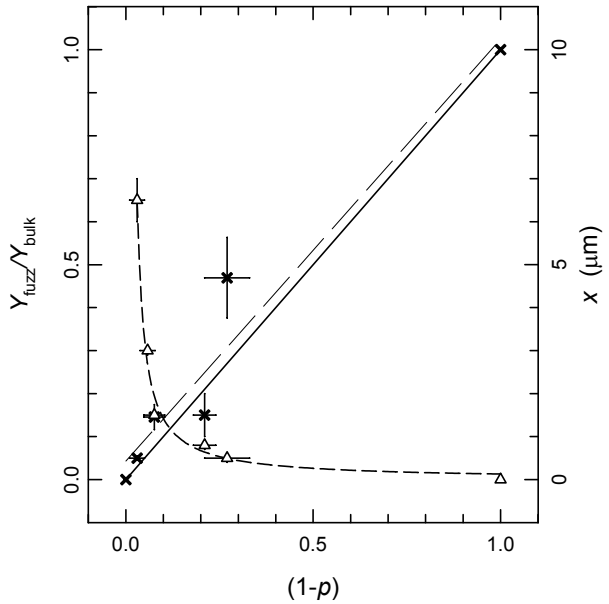

Figure C1. Plot of $Y_{\text{fuzz}}/Y_{\text{bulk}}$ (crosses) and x (triangles), versus $(1-p)$: a re-plot of figure 6(a) in [10] and a few more recent data. Fitted lines are discussed in the text.

References

[1] M.J. Baldwin and R.P. Doerner. Helium induced nanoscopic morphology on tungsten under fusion relevant plasma conditions. *Nuclear Fusion*, 48:035001, 2008.

[2] S. Kajita, W. Sakaguchi, N. Ohno, N. Yoshida, and T. Saeki. Formation process of tungsten nanostructure by the exposure to helium plasma under fusion relevant plasma conditions. *Nuclear Fusion*, 49:095005, 2009.

[3] M.J. Baldwin, T.C. Lynch, R.P. Doerner, and J.H. Yu. Nanostructure formation on tungsten exposed to low-pressure rf helium plasmas: A study of ion energy threshold and early stage growth. *Journal of Nuclear Materials*, 415(1, Supplement):S104 – S107, 2011.

[4] T.J. Petty and J.W. Bradley. Tungsten nanostructure formation in a magnetron sputtering device. *Journal of Nuclear Materials*, 453(1-3):320–322, 2014.

[5] S. Kajita, N. Yoshida, R. Yoshihara, N. Ohno, and M. Yamagiwa. Tem observation of the growth process of helium nanobubbles on tungsten: Nanostructure formation mechanism. *Journal of Nuclear Materials*, 418:152 – 158, 2011.

[6] M.J. Baldwin, R.P. Doerner, D. Nishijima, K. Tokunaga, and Y. Ueda. The effects of high fluence mixed-species (deuterium, helium, beryllium) plasma interactions with tungsten. *Journal of Nuclear Materials*, 390-391(0):886 – 890, 2009.

[7] Y Noiri, S Kajita, and N Ohno. Nanostructure growth by helium plasma irradiation to tungsten in sputtering regime. *Journal of Nuclear Materials*, 2015.

[8] M.J. Baldwin and R.P. Doerner. Formation of helium induced nanostructure fuzz on various tungsten grades. *Journal of Nuclear Materials*, 404(3):165 – 173, 2010.

[9] S. Takamura, N. Ohno, D. Nishijima, and S. Kajita. Formation of nanostructured tungsten with arborescent shape due to helium plasma irradiation. *Plasma and Fusion Research*, 1:051–051, 2006.

[10] D. Nishijima, M.J. Baldwin, R.P. Doerner, and J.H. Yu. Sputtering properties of tungsten fuzzy surfaces. *Journal of Nuclear Materials*, 415(1, Supplement):S96 – S99, 2011.

[11] S. Kajita, N. Yoshida, R. Yoshihara, N. Ohno, T. Yokochi, M. Tokitani, and S. Takamura. Tem analysis of high temperature annealed w nanostructure surfaces. *Journal of Nuclear Materials*, 421(13):22 – 27, 2012.

[12] R.P. Doerner, M.J. Baldwin, and P.C. Stangeby. An equilibrium model for tungsten fuzz in an eroding plasma environment. *Nuclear Fusion*, 51:043001, 2011.

[13] K. Tokunaga, R.P. Doerner, R. Seraydarian, N. Noda, Y. Kubota, N. Yoshida, T. Sogabe, T. Kato, and B. Schedler. Surface morphology and helium retention on tungsten exposed to low energy and high flux helium plasma. *Journal of Nuclear Materials*, 313-316(0):92 – 96, 2003.

[14] K Tokunaga, S Tamura, N Yoshida, K Ezato, M Taniguchi, K Sato, S Suzuki, and M Akiba. Synergistic effects of high heat loading and helium irradiation of tungsten. *Journal of Nuclear Materials*, 329-333, Part A(0):757 – 760, 2004.

[15] S. Takamura, T. Miyamoto, and N. Ohno. Effects of fibre-form nanostructures on particle emissions from a tungsten surface in plasmas. *Nuclear Fusion*, 52(12):123001, 2012.

[16] S. Kajita, N. Ohno, M. Yajima, and J. Kato. Growth annealing equilibrium of tungsten nanostructures by helium plasma irradiation in non-eroding regimes. *Journal of Nuclear Materials*, 440(1-3):55–62, September 2013.

[17] Y. Ueda, K. Miyata, Y. Ohtsuka, H.T. Lee, M. Fukumoto, S. Brezinsek, J.W. Coenen, A. Kreter, A. Litnovsky, V. Philipps, B. Schweer, G. Sergienko, T. Hirai, A. Taguchi, Y. Torikai, K. Sugiyama, T. Tanabe, S. Kajita, and N. Ohno. Exposure of tungsten nano-structure to textor edge plasma. *Journal of Nuclear Materials*, 415(1, Supplement):S92 – S95, 2011.

[18] G.M. Wright, D. Brunner, M.J. Baldwin, R.P. Doerner, B. Labombard, B. Lipschultz, J.L. Terry, and D.G. Whyte. Tungsten nano-tendril growth in the alcator c-mod divertor. *Nuclear Fusion*, 52(4):042003, 2012.

[19] S.I Krasheninnikov. Viscoelastic model of tungsten fuzz growth. *Physica Scripta*, T145:014040,

December 2011.

[20] K.J. Taylor, S. Yuna, and G.R. Tynan. Control of plasma parameters by using noble gas admixtures. *Journal of Vacuum Science & Technology A: Vacuum, Surfaces, and Films*, 22(5):2131, 2004.

[21] D.M. Goebel, G. Campbell, and R.W. Conn. Plasma surface interaction experimental facility (PISCES) for materials and edge physics studies. *Journal of Nuclear Materials*, 121:277–282, 1984.

[22] Y. Hirooka. A new plasma-surface interactions research facility: PISCES-B and first materials erosion experiments on bulk-boronized graphite. *Journal of Vacuum Science & Technology A: Vacuum, Surfaces, and Films*, 8(3):1790, May 1990.

[23] S. Kajita, T. Saeki, Y. Hirahata, M. Yajima, N. Ohno, R. Yoshihara, and N. Yoshida. Development of nanostructured black metal by self-growing helium bubbles for optical application. *Japanese Journal of Applied Physics*, 50(8):08JG01, 2011.

[24] W. Eckstein. *Calculated sputtering, reflection and range values.* IPP 9. Max-Planck-Institut für Plasmaphysik, 2002.

[25] H.T. Lee, A.A. Haasz, J.W. Davis, and R.G. Macaulay-Newcombe. Hydrogen and helium trapping in tungsten under single and sequential irradiations. *Journal of Nuclear Materials*, 360(2):196 – 207, 2007.

[26] H Iwakiri, K Yasunaga, K Morishita, and N Yoshida. Microstructure evolution in tungsten during low-energy helium ion irradiation. *Journal of Nuclear Materials*, 283287, Part 2(0):1134 – 1138, 2000.

[27] O El-Atwani, S Gonderman, S Suslov, M Efe, G De Temmerman, T Morgan, K Bystrov, K Hattar, and J P Allain. Early stage damage of ultrafine-grained tungsten materials exposed to low energy helium ion irradiation. *Fusion Engineering and Design*, pages 1–6, 2015.

[28] M.J. Baldwin, R.P. Doerner, W.R. Wampler, D. Nishijima, T. Lynch, and M. Miyamoto. Effect of he on d retention in w exposed to low-energy, high-fluence (d, he, ar) mixture plasmas. *Nuclear Fusion*, 51(10):103021, 2011.

[29] R. M. Corless, G. H. Gonnet, D. E. G. Hare, D. J. Jeffrey, and D. E. Knuth. On the Lambert W function. *Advances in Computational Mathematics*, 5:329–359, 1996.

[30] D. Nishijima, R.P. Doerner, M.J. Baldwin, and G. De Temmerman. Erosion yields of deposited beryllium layers. *Journal of Nuclear Materials*, 390391(0):132 – 135, 2009.

[31] R.P. Doerner, C. Bjrkas, D. Nishijima, and T. Schwarz-Selinger. Erosion of beryllium under high-flux plasma impact. *Journal of Nuclear Materials*, 438, Supplement(0):S272 – S275, 2013.

[32] J.N. Brooks, J.P. Allain, R.P. Doerner, A. Hassanein, R. Nygren, T.D. Rognlien, and D.G. Whyte. Plasma-surface interaction issues of an all-metal ITER. *Nuclear Fusion*, 49(3):035007, March 2009.

[33] H. Bolt, V. Barabash, W. Krauss, J. Linke, R. Neu, S. Suzuki, and N. Yoshida. Materials for the plasma-facing components of fusion reactors. *Journal of Nuclear Materials*, 329-333:66–73, 2004.

[34] Joachim Roth, E. Tsitrone, and A. Loarte. Recent analysis of key plasma wall interactions issues for ITER. *Journal of Nuclear Materials*, 390-391:1–9, June 2009.

[35] R.a. Pitts, S. Carpentier, F. Escourbiac, T. Hirai, V. Komarov, S. Lisgo, A.S. Kukushkin, A. Loarte, M. Merola, A. Sashala Naik, R. Mitteau, M. Sugihara, B. Bazylev, and P.C. Stangeby. A full tungsten divertor for ITER: Physics issues and design status. *Journal of Nuclear Materials*, 438:S48–S56, January 2013.

[36] Y. Igitkhanov, B. Bazylev, and R. Fetzer. *The quantification of the key physics parameters for the DEMO fusion power reactor and analysis of the reactor relevant physics issues.* KIT Scientific Reports. 2015.

[37] R.M. Corless, G.H. Gonnet, D.E.G. Hare, D.J. Jeffrey, and D.E. Knuth. On the lambert w function. *Advances in Computational Mathematics*, 5(1):329–359, 1996.